GEOMETRY EFFECTS ON FLOW PATTERN AND WALL SHEAR STRESS IN HUMAN INTERNAL CAROTID ARTERIES

A. Sharifi [1], H. Niazmand [2]

[1]M.SC. Student, Ferdowsi university of Mashhad; Sharifialireza@yahoo.com

[2]Professor, Ferdowsi university of Mashhad; niazmand@um.ac.ir

Abstract

Worldwide, stroke is the second leading cause of death, responsible for 4.4 million (9 percent) of the total 50.5 million deaths each year. More than 4 million people in the United States have survived a stroke or brain attack and are living with the aftereffects. It has been reported that the carotid siphon is the site most susceptible to atherosclerotic lesions in the human intracranial arteries, directly affecting the cerebral blood supply. The relatively complex geometry containing out of plane curves has a great impact on the associated hemodynamic, which plays a significant role on the atherogenesis. There are medical reports that indicate atherosclerotic stenoses is widely observed in different sites of internal carotid artery (ICA). Relatively few studies have examined the geometrical features of these arteries to identify regions of low or oscillatory shear stress that contributes to atherogenesis. However, there are still some conflictions about risky sites in these arteries, which require further studies. Furthermore, previous studies include some simplifications especially on the blood flow profiles that bring some uncertainties regarding their findings. Therefore, the purpose of the present study is to investigate the blood flow patterns in ICA to identify the risky sites prone to atherosclerosis. Geometrical models are made based on the clinical studies about the classification of internal carotid siphon geometry. Three different geometries of the ICA were simulated by Open source CFD software Open FOAM. In the present study, flow patterns and wall shear stresses have been examined extensively and the preferred sites of stenoses along the carotid siphon of the different geometries of the ICA are identified.

Keywords: Internal carotid artery, Carotid siphon, hemodynamic, Open Foam, Stenosis

Introduction

Evidence gathered in the recent decades supports theidea that the formation and development of arterialstenoses are the result of a complex interplay between systemic factors, changes in the biomechanical propertiesof vessel walls, and local hemodynamic factors such as lowand oscillatory wall shear stress (Varghese and Frankel, 2003). It has been reported that the carotid siphon is the site most susceptible to atherosclerotic lesions in the human intracranial arteries, directly affecting the cerebral blood supply (Reneman and Hoeks, 2008).Therefore, understanding blood flow patterns in ICAs with different geometries can lead to the

identification of patients vulnerable to atherosclerosis. Atherosclerosis is a disease in which plaque builds up inside the arteries. Plaque is made up of fat, cholesterol, calcium, and other substances found in blood. Over time, plaque hardens and narrows the artery, which limits the flow of oxygen-rich blood to organs and other parts of body (Yagi, 1998).Among many curved arteries in human body the internal carotid artery (ICA) is more prone to atherosclerosis.The common carotid artery is found bilaterally on each side of the anterior neck. Each common carotid artery is divided into an external and internal carotid artery. The external carotid artery supplies blood to structures outside the skull, primarily the face, and the internal carotid to structures inside the skull, including the brain. The external carotid artery is straight, but the internal carotid artery twists and turns, increasing the likelihood of blockages. A severe blockage may cause a stroke byreducing blood flow to the brain(Gibo et al., 1981).

Several investigations have been done to gather more information about mechanical features of blood in ICA. In primary studies, arteries have been modeled by simple curves (45 and 90 degree curves) like what has been done by Chang (Chang and Tarbell, 1985) in which Sinusoidal and pulsatile flow in curved tubes was simulated. In recent studies models were improved and the real shape of these arteries were reconstructed and it observed that ICA has different shapes, but just blood flow in two shapes of these arteries were computationally studied (Qiao et al., 2004; Oshima et al., 2005). All of these studies have shown that the flow pattern in long curves is complex and non-uniform so it can affect the function of arterial endothelium. To have results much more close to the reality, 4D MRI imaging technology were used to visualize the blood flow in ICA in vivo, and found very complex flow with helical and twisting patterns in carotid siphon (Wetzel et al., 2007; Bammer et al., 2007). Medical images were reconstructed from the original by Sforza et al. (2009), wall shear stress (WSS) in the ICA siphon computationally was evaluated and found to be relatively low compared to the other cerebral arteries. Zhang et al. (2013) has performed a comprehensive study to classify the ICA shapes and provided four ideal models based on the average physical features and dimensions. In their numerical simulation of these models only wall shear stress distributions were examined for a sinusoidal velocity inlet and constant pressure outlet. A similar study has been conducted by Zhang et al. (2012) with a more realistic pressure outlet condition to provide more information about flow patterns and effective parameters in ICA stenosis. Although these studies provide useful information about ICA arteries, yet there is still room for the investigation of the complex flow patterns in the ICA siphon. Therefore, in the present study the flow patterns in three idealized ICA models have been investigated with a realistic inlet velocity and pressure outlet as presented in figure 4. Since Ideal models are based on the averaged geometric parameters of each type of ICA, they are more suitable for parametric studies as compared to patient specific models.

The time variations of the axial velocity profiles and cross sectional contours are examined in relatively more risky sites. Furthermore, the time averaged wall shear stress distributions during a cardiac cycle are provided to identify the locations, which are more prone to the formation of the atherosclerotic plaques.

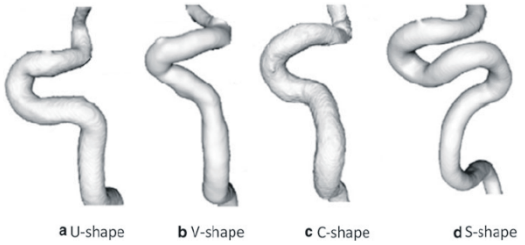

Fig. 1. Examples of carotid siphon shape classes (Zhang et al., 2013)

Physical models:

According to the anatomic classification of the siphon, the ICA shape can be classified into 4 types: U-, V-, C- and S-shape as shown in figure 1 (Zhong et al., 1985). However, most of the cases are of U, V and C shape, and therefore, have attracted more attention. In the present study physical models are constructed following the information provided by Zhang et al., 2013 as presented in figure 2. All models consist of different non-planar bends with different curve angels and curvature radius. Although the bend shapes in V model look very much the same as those in C model, the strong non-planar bends in C model cause more complicated flow patterns as will be discussed later.

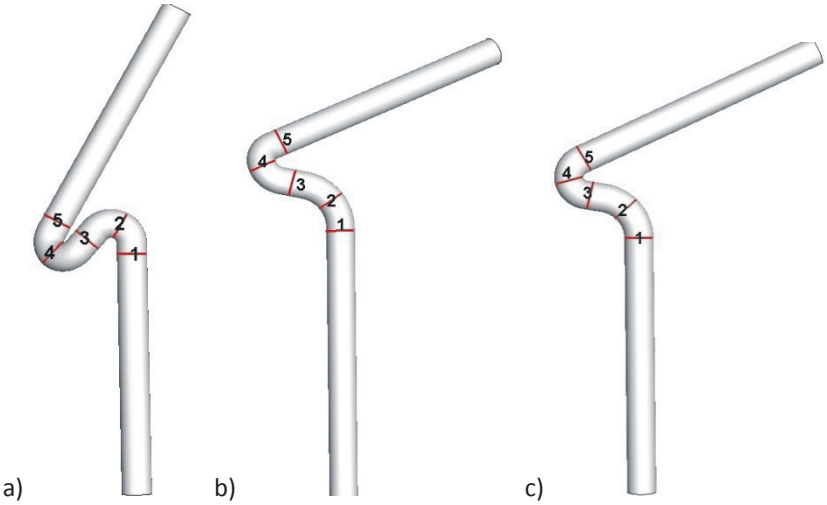

Fig. 2. Three types of internal carotid artery a: U type, b: V type, c: C type

ICA bends are also named according to their geometrical features and location. B1 is the second bend, which is also called the anterior knee of the siphon and B2 is the first bend located in the posterior knee of the siphon.

Numerical Method

A structured mesh is used for all models, which are relatively finer near the wall to resolve the local higher gradients. Extensive computations have been performed to identify the number of grid points that produce reasonably grid-independent results. It was found the minimum grid points of 40, 21, 135 are required in the

azimuthal, radial, and axial directions, respectively. Uniform grid spacing is used in the azimuthal direction, while the expansion ratio of 1.10 is employed in the radial direction. The inlet and outlet are set perpendicular to the centerline of the ICA models. The outlet is located far enough away from the siphon to accurately model the zero velocity gradients applied at this boundary. The unsteady nature of the flow is applied by the realistic velocity wave form at the inlet and pressure at the outlet taken from Ho et al. (2010) as shown in the figure 3 and 4.

The blood was considered as incompressible Newtonian fluid with density of ρ=1056 kg/m3 and dynamic viscosity of $\mu=4\times10^{-3}$kg/ms. The blood vessel walls are considered rigid with non-slip condition(Lee et al., 2008). According to the ICA inside diameter, the peak Reynolds number varies between 364 and 428 and therefore, the flow is laminar.

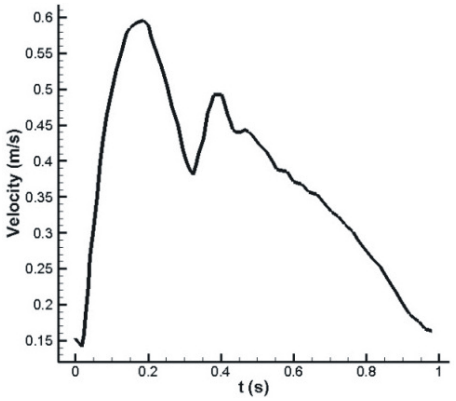

Fig. 3. Real velocity pulse of blood at the inle

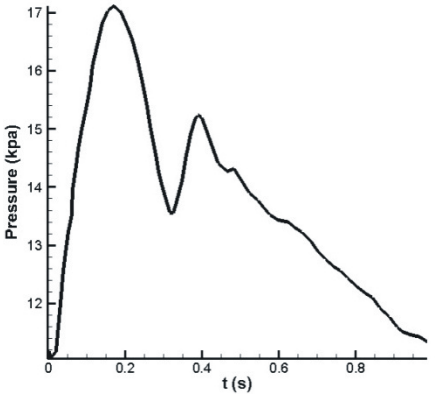

Fig. 4. Real pressure pulse of blood at the outlet

Governing equations

The governing equations can be expressed as:

Continuity equation

$$\vec{\nabla} \cdot \vec{V} = 0$$

Navier–Stokes equation

$$\rho(\frac{\partial \vec{V}}{\partial t} + \vec{V}.\vec{\nabla}\vec{V}) = -\vec{\nabla}P + \mu\nabla^2\vec{V}$$

$\vec{V}$ Is the blood flow velocity and P is the pressure. Flow is simulated with the finite volume OpenFOAM software using a second-order unsteady solver PimpleFOAM, which works based on Pimple algorithm. As the cycle of the pulsatile flow is 0.8s, the time step was set to 1e-4s to obtain relatively time accurate results. At least six cycles are required to reach cyclic accurate resolution.

Results

To gain a global view of the velocity field variations through the bends a magnified view of three dimensional velocity profiles are presented for a U shape model in figure 5. The chosen cross sections are related to the bends, where velocity profiles undergo considerable changes. The figure shows that the relatively parabolic velocity profile at the bend inlet transforms to a very complicated profile at the first bend due to the centrifugal forces and the non-planarity of the bend. The point of maximum velocity moves towards the outer bend with a small back flow region located in the inner bend. In cross section 3 this reverse flow region extends and the centrifugal effects are more clear as the location of the maximum cross sectional velocity complies with the first bend. In cross section 4 the velocity profile is still under the effect of the first bend and the maximum velocity is located in the inner bend region. The complex velocity profile after the second bend is affected by the successive bends and the non-planarity of the exit section. The surface pressure distribution is also included, where the local maximum pressure in outer region of the first bend is responsible for the formation of the crescent velocity profile in this section.

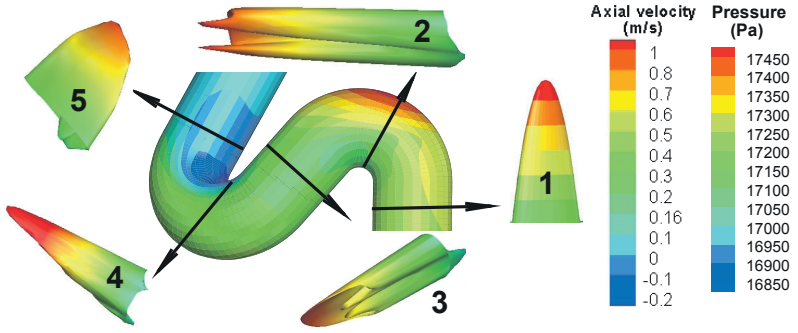

Fig. 5. Three dimensional axial velocity profiles along the U type model and its surface pressure distribution at 0.2 s.

Five cross sections along the ICA siphon as shown in figure 2 are chosen to represent the detailed cross sectional velocity contours and axial velocity profiles. Furthermore, in figure 6 the lines along which the axial velocity profiles are plotted (in figures 8-10) are shown. Lines A and B are located in the first and second bend (cross sections 2 and 4 in figure 6), which are commonly called B2 and B1,

respectively. Line C is located in the fifth cross section of all models. In addition to the axial velocity contours, streamlines related to the secondary flow field at time 0.2s are plotted in figure 7 for all three models and mentioned cross sections. As can be seen in figure 3, time 0.2s corresponds to the systole point, where the velocity is maximized.

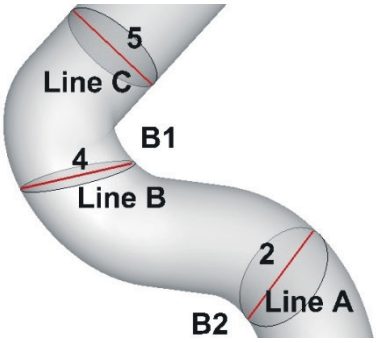

Fig. 6. Line locations in ICA siphon (Line A, B and C), bend names (B2 is the first bend and B1 in the second bend)

In the first cross section of all models, the axial flow is almost fully developed, while primary effects of the bend create a relatively weak secondary flow from the outer to the inner region. In B2 bend cross section, as visible in figure7, a2, b2, c2, Dean Structures form, which helps the formation of the crescent shape in the axial velocity profiles displacing the maximum axial velocity region towards the outer bend. Clearly, the centers of the Dean

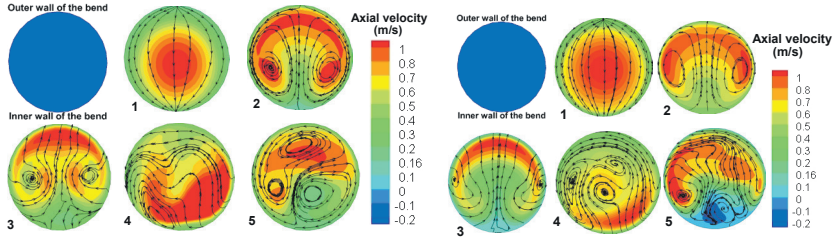

a: U shape b: V shape

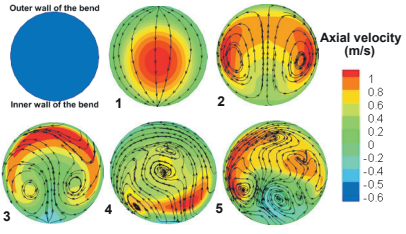

c: C shape

Fig. 7. Streamlines of secondary in-plane flow are overlaid on contours of axial velocity, at different locations of the ICA siphon at t=0. 2 s for the U-, V-and C-shaped cases. a: U-shape, b:V-shape and c: C-shape; (1) plane1, (2)plane2, (3)

plane3, (4) plane4 and (5) plane5. All slices are orientated so that the top of the slice is the top of the model.

Vortexes in Figure 7 a2 corresponds to the two local maximum axial velocity points in Figure 5 section 2 of the U shape model.

In cross section 3 of all models, figure 7 a3, b3, and c3 the strong centrifugal effects of the B2 bend are still present with the axial crescent profile, which is relatively limited to the wall region. However, the slight reverse flow region is apparent for V and C shape models as will discuss with respect to figure 8 in more details.

The flow in the second bend of all models is more interesting. Curvature variations upon entering the second bend have distinct effects on the flow, as the peak in the flow profile begins to move toward the lower wall, a4, b4, c4 figure7. Yet, the flow structure in this cross section and in cross section 5 is very complicated due to the successive bends and their non-planarity effects.

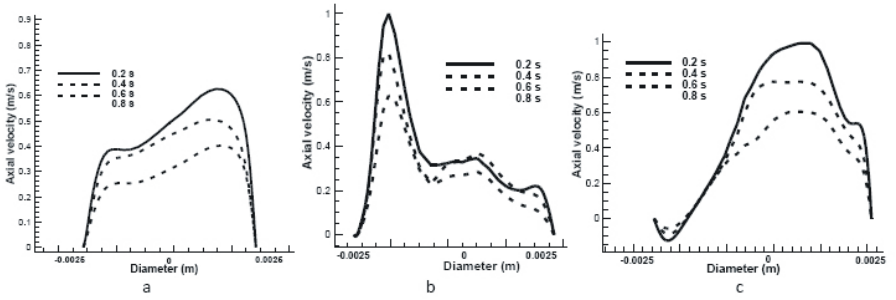

Fig. 8. Axial velocity profiles at different times for U type model on line A, B and C

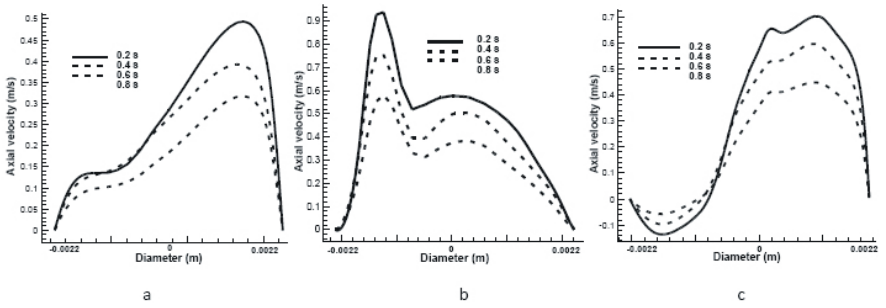

Fig. 9. Axial velocity profiles at different times for V type model on line A, B and C

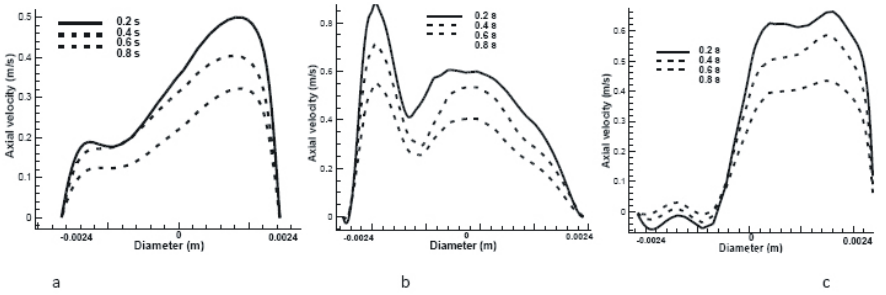

Fig. 10. Axial velocity profiles at different times for C type model on line A, B and C

To capture a sense of the time variation of the flow field, In figures 8, 9, and 10 the axial velocity profiles along the A, B, and C lines (from the inner towards outer) as shown in figure 6 at different times are presented for all three models. Clearly, the axial velocity profiles in V and C models are almost the same for A and B lines due to their geometrical similarities. However, considerable differences are observed in their C line profiles and all velocity profiles of the U shape model. The solid line in all figures corresponds to the 0.2s in the cycle time, where the cross sectional profiles are also shown in figure 7a-b- and c. Velocity profiles along the C line of all models indicate a reverse flow region during the whole cycle time, which is more pronounced in the V shape model. The extent of the reverse flow region throughout the cross section at time 0.2 is more clear in figure 7 a5, b5, c5 the in the inner part of the B1 bend. Experiencing negative velocities makes this region to be of the most preferred sites for stenoses. The fact that the V shape model is more prone to stenosis is also supported by the finding of Zhang.

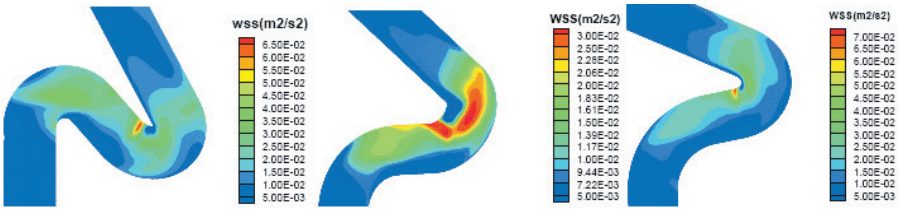

Fig. 11. Wall shear stress distribution on the ICA siphon wall for a: U type, b: V type and c: C type

In addition to velocity profiles the wall shear stresses are good indicators of the sites susceptible to stenosis. In Figure 11 wall shear stress contours along the ICA siphon in different models are presented at time 0.2s of the cycle. Base on the above results, regions of low wall shear stresses, which are also included the reverse flow regions are the outer of B2 and B1 and the inner of the B1 downstream. These sites are more susceptible to atherosclerotic lesions, however, the exact locations and their extensions vary between three types of the ICA. The inner parts of B2 and B1 in V type always face the negative velocity and experiences much lower wall shear stresse, which increases the risk of stenosis in these parts.

Conclusion

Three different geometries of the ICA were simulated by Open source CFD software Open FOAM to investigate the blood flow patterns in ICA to identify the risky sites prone to atherosclerosis. Realistic inlet velocity and pressure outlet is used at the inlet and outlet of the arteries, flow patterns and wall shear stresses have been examined extensively. The preferred sites of stenoses along the carotid siphon of the different geometries of the ICA are generally identified as the inner of B2 and B1 and the inner of the B1 downstream for all three models and especially the inner parts of B2 and B1 in V type.

References:

VARGHESE, S. S. & FRANKEL, S. H. 2003. Numerical modeling of pulsatile turbulent flow in stenotic vessels. *Journal of biomechanical engineering,* 125**,** 445-460.

YAGI, K. 1998. Simple procedure for specific assay of lipid hydroperoxides in serum or plasma. *Free radical and antioxidant protocols.* Springer.

GIBO, H., LENKEY, C. & RHOTON JR, A. L. 1981. Microsurgical anatomy of the supraclinoid portion of the internal carotid artery. *Journal of neurosurgery,* 55**,** 560-574.

RENEMAN, R. S. & HOEKS, A. P. 2008. Wall shear stress as measured in vivo: consequences for the design of the arterial system. *Medical & biological engineering & computing,* 46**,** 499-507.

HO, H., LADD, D., HOLDEN, A. & HUNTER, P. 2010. Patient-Specific Hemodynamic Analysis for Proximal Protection in Carotid Angioplasty. *Computational Biomechanics for Medicine.* Springer.

CHANG, L.J., TARBELL, J.M., 1985. Numerical simulation of fully developed sinusoidal and pulsatile (physiological) flow in curved tubes*. Journal of Fluid Mechanics* 161, 175–198.

QIAO, A.K., GUO, X.L., WU, S.G., ZENG, Y.J., Xu, X.H., 2004. Numerical study of nonlinear pulsatile flow in S-shaped curved arteries. *Medical Engineering & Physics* 26, 545–552.

WETZEL, S., MECKEL, S., FRYDRYCHOWICZ, A., BONATI, L., RADUE, E.W., SCHFFLER, K., HENNING, J., MARKL, M., 2007. In vivo assessment and visualization of intracranial arterial hemodynamic with flow-sensitized 4D MR imaging at 3T. *American Journal of Neuroradiology* 28, 433–438.

SFORZA, D.M., PUTMAN, C.M., CEBRAL, J.R., 2009. Hemodynamic of cerebral aneurysms. *Annual Review of Fluid Mechanics* 41, 91–107.

ZHONG, S.Z., HAN, Y.J., YEN, W.C., 1985. *Microsurgical Anatomy*. MTP Press, Boston.

ZHANG, C., PU, F., LI, S., XIE, S., FAN, Y. & LI, D. 2013. Geometric classification of the carotid siphon: association between geometry and stenoses. *Surgical and Radiologic Anatomy,* 35**,** 385-394.

ZHANG, C., XIE, S., LI, S., PU, F., DENG, X., FAN, Y. & LI, D. 2012. Flow patterns and wall shear stress distribution in human internal carotid arteries: the geometric effect on the risk for stenoses. *Journal of biomechanics,* 45**,** 83-89.

Lee, S.E., LEE, S.W., FISCHER, P.F., BASSIOUNY, H.S., LOTH, F., 2008. Direct numerical simulation of transitional flow in a stenosed carotid bifurcation. *Journal of Biomechanics* 41, 2551–2561.